Received: 5 January 2023 | Revised: 8 February 2023 | Accepted: 30 March 2023
DOI: 10.1002/apj.2915

RESEARCH ARTICLE

Asia-Pacific Journal of Chemical Engineering | Curtin University | WILEY

# Preparation of calcium sulfide by sludge-assisted rice husk reduction of phosphogypsum

**Dong Ma** | **Qinhui Wang** | **Zhihua Tian**

State Key Laboratory of Clean Energy Utilization, Institute for Thermal Power Engineering, Zhejiang University, Hangzhou, 310027, China

**Correspondence**
Qinhui Wang, State Key Laboratory of Clean Energy Utilization, Institute for Thermal Power Engineering, Zhejiang University, Hangzhou 310027, China.
Email: qinhui__wang@126.com

**Funding information**
school-enterprise cooperation projects, Grant/Award Number: 2019-KYY-508101-0078

**Abstract**

Reduction of phosphogypsum (PG) to calcium sulfide (CaS) using thermochemical methods solve the environmental problems caused by PG. However, the commonly used reducing agents are coal and CO. The use of the above-mentioned reducing agents is not economically efficient. In this paper, rice husk (RH) is used as a reducing agent and sludge (SL) as an additive to reduce PG. The effect of the two on PG decomposition and the mechanism of the synergistic effect are also investigated in combination with kinetic calculations. It is found that decomposition rate of $CaSO_4$ in PG is 99.99% and yield of CaS is 98.38% when 40% RH + 20% SL is used as the reducing agent at 900°C for 30 min. The combined use of RH + SL is superior to RH alone in reducing the initial decomposition temperature and $E_a$. The mechanism functions of both reduced PG are $G(\alpha) = -\ln(1-\alpha)$. There is a synergistic mechanism between RH and SL. The $Fe_2O_3$ in SL increases the cleavage of nitrogen oxide-containing compounds and PAHs in tar to monocyclic aromatic and aliphatic hydrocarbons while producing more CO, $H_2$, and $CH_4$. Meanwhile, SL ash can promote the reaction process of carbon with $CaSO_4$, thus increasing the decomposition rate of PG.

**KEYWORDS**

CaS, phosphogypsum, reduction, rice husk, sludge

## 1 | INTRODUCTION

Phosphogypsum (PG) is a byproduct of phosphorus chemical firms when producing phosphoric acid. The production of the PG industry in China is 75.1 million tons in 2022, and the total usage is 36 million tons. Only 47.9% of the capacity is being utilized.[1] $CaSO_4 \cdot nH_2O$ ($n = 0$, 0.5, 1.5, 2) is the primary constituent of PG. Additionally, it contains a variety of impurities like Si, Fe, Mg, Al, P, and F, as well as organic debris and trace metals like Cr and Pb.[2] Due to the high number of impurities and a certain degree of radiation, the large-scale application of PG is severely limited. At present, PG is mainly disposed of by stockpiling.[3] In addition to taking up a significant amount of space, piling PG also easily results in air and groundwater pollution. Therefore, the PG problem has become a major pain point for wet process phosphoric acid production.[4] In summary, the treatment of PG is urgently needed.

The use of thermochemical methods to convert PG to calcium sulfide (CaS) can effectively mitigate the environmental problems caused by PG. CaS as an intermediate product can continue roasting with PG at high temperatures to produce lime slag and sulfur dioxide. First of all, it can alleviate the environmental pollution caused by PG.[5] In addition, the generated lime slag can be used for construction materials, acidic sewage treatment, calcium carbonate whiskers, and soil utilization.[6]

Sulfur dioxide can be used to make organic solvents and refrigerants. In addition, CaS can be used to prepare fluorescent materials and insecticides, and so forth.[7]

The type of reducing agent and the C/Ca molar ratio are the two most important factors influencing PG decomposition. The common reducing agents used for PG reduction mainly include solid reducing agents such as lignite,[8,9] anthracite,[10] high sulfur coal,[11] coke,[12] and gaseous reducing agents such as CO,[13] $H_2$,[14] and $H_2S$.[15] It is shown that pure graphite hardly reacted with $CaSO_4$, while coal and char could effectively decompose PG. Moreover, when other conditions are the same, the PG decomposition rates of coals with low degrees of metamorphism (lignite and bituminous coal) are significantly better than those of coals with higher degrees of metamorphism (anthracite). This is due to the fact that the ash in coal played a catalytic role in PG decomposition. The $Fe_2O_3$ in coal can effectively promote the decomposition of PG. The C/Ca molar ratio not only has an important effect on PG decomposition products but also affects the decomposition temperature of PG. Through experiments, Zhang et al.[16] discovered that adding lignite under $CO_2$ lowered the breakdown temperature of PG. Additionally, as the amount of lignite increased, the decomposition temperature gradually reduced. When $n_C/n_{Ca}$ is 2, the main product is CaS. With the decrease of carbon injection, CaS is gradually converted to CaO. However, the use of the above-mentioned reducing agents is not economically efficient. Currently, solid sites such as olive processing sitewater,[17] petroleum coke,[12] and coal gangue[18] are used as reducing agents, which can reduce economic costs as well as meet "dual carbon" requirements.

Rice husk (RH), as a by-product of rice processing production, is discarded, composted, or burned as agricultural site in large quantities, resulting in energy site as well as environmental pollution. Since RH contains high volatile fraction and low sulfur content,[19] reducing PG to CaS by pyrolysis of RH to produce CO, $CH_4$, and $H_2$ gases not only solves the environmental pollution problem but also produces CaS to prepare CaO. However, lignin in RH is more difficult to decompose during pyrolysis, and catalytic pyrolysis by adding catalysts to RH can both promote the decomposition of lignin and produce more reducing gases.[20] Sludge (SL) is the main site material in sitewater treatment process, which has the characteristics of high ash and sulfur content. Using SL pyrolysis not only can generate reducing gases to reduce PG, but also SL contains many metal oxides such as $Fe_2O_3$, MgO, CaO, and $Al_2O_3$, and most of these metal-based compounds have a positive contribution to the effect of the pyrolysis process because of their multivalent state and acidic sites.[21] Gao et al.[22] found that the main active components (CaO, $SiO_2$, and $Fe_2O_3$) in SL greatly contributed to the tar cracking effect, leading to a significant increase in gas content. This suggests that SL can assist RH pyrolysis to improve gas production.

In summary, this paper investigates the effect and mechanism of the synergistic effect of CaS as the target product, RH as the reducing agent and SL as the additive on the decomposition of PG, combined with kinetic calculations. The study provides ideas for developing more economically and environmentally efficient reductant decomposition of PG.

## 2 | EXPERIMENTAL

### 2.1 | Raw materials

PG is from a phosphorus chemical company. It is dried for 6 h at 105°C and then kept for backup. Chemical composition of the dried PG is analyzed by X-ray fluorescence spectrometer (XRF, Shimadzu XRF-1800, Japan) as shown in Table 1. Contents of CaO and $SO_3$ in PG are 33.51% and 47.87%, respectively. It also contained 17.25% $SiO_2$ and small amounts of $Fe_2O_3$, $Al_2O_3$, $P_2O_5$, F, and organic matter. The physical phase analysis of PG is performed using X-ray diffraction (XRD) as shown in Figure S1. The dried PG is mainly composed of $CaSO_4$, $SiO_2$, and $CaSO_4{\cdot}0.5H_2O$. Using a particle size analyzer (Zetasizer Nano S90 Malvern), the average PG particle size is found to be 40.8 μm.

RH is purchased from a grain and oil factory in Jiangsu, China. SL is obtained from a printing and dyeing industrial wastewater treatment plant in China. The RH and SL are crushed and sieved to get a powder measuring 0.125–0.25 mm, which is then dried at 105°C for 6 h and kept as a backup. Industrial analysis tests of RH and SL are performed with GB/T 212-2008. Elemental analysis tests of RH and SL are performed with GB/T 31391-2015. Table 2 summarizes the findings of industrial and elemental analysis of dried RH and SL. The SL is fully calcined at 900°C for 6 h to prepare sludge ash (SLA). SLA is analyzed for chemical composition with XRF, and Table 3 summarizes the SLA composition. According to Tables 2 and 3, the fixed carbon and volatile content of RH is much larger than that of SL. The ash concentration of SL can reach 54.02%, with $SiO_2$, $Fe_2O_3$, $Al_2O_3$, and CaO dominating.

### 2.2 | Experimental method

Figure S2 depicts the experimental setup, which is a rapid warming fixed bed reactor. Experiments are carried out

**TABLE 1** Ingredients in PG (%).

| CaO | $SO_3$ | $SiO_2$ | $Fe_2O_3$ | $Al_2O_3$ | $K_2O$ | MgO | $P_2O_5$ | Total F | Organic matter |
|---|---|---|---|---|---|---|---|---|---|
| 33.51 | 47.87 | 17.25 | 0.54 | 0.51 | 0.23 | 0.25 | 0.58 | 0.20 | 0.30 |

**TABLE 2** Main characteristics of samples.

| | Industrial analysis, % | | | | Elemental analysis, % | | | | |
|---|---|---|---|---|---|---|---|---|---|
| Sample | $M_{ad}$ | $A_{ad}$ | $V_{ad}$ | $FC_{ad}$ | $C_{ad}$ | $H_{ad}$ | $O_{ad}$ | $N_{ad}$ | $S_{t,ad}$ |
| RH | 2.31 | 10.55 | 68.27 | 18.87 | 45.39 | 5.24 | 36.0 | 0.31 | 0.20 |
| SL | 6.36 | 54.02 | 33.13 | 6.49 | 13.49 | 1.55 | 19.61 | 2.04 | 2.93 |

*Note*: $M_{ad}$, moisture (air dry basis); $A_{ad}$, ash (air dry basis); $V_{ad}$, volatile matter (air dry basis); $FC_{ad}$, fixed carbon (air dry basis).

**TABLE 3** Ash composition of SL (%).

| $SiO_2$ | $Fe_2O_3$ | $Al_2O_3$ | CaO | $SO_3$ | $Na_2O$ | MgO | $K_2O$ |
|---|---|---|---|---|---|---|---|
| 32.39 | 24.12 | 14.50 | 9.37 | 7.25 | 1.53 | 1.51 | 1.29 |

in the order shown below. First, a certain mass of reactants is weighed and deposited in the quartz tube's low temperature region. Following further warming to the required temperature, the sample is instantly put into the reactor's thermostatic portion to begin the reaction. In the experiment, the flow rate of $N_2$ is set at 200 mL/min. The pyrolysis barren gas enters the two-stage condenser tube, and the refrigerant in the shell layer of the cooling tube is ethylene glycol aqueous solution, and the circulating cooling temperature is $-10^\circ C$. After the cooling, the tar-containing mist gas is absorbed by acetone in turn. The gas is collected by gas bag. The solid product after cooling is weighed and stored.

## 2.3 | Kinetic calculations

Thermogravimetric experiments are performed on STA 449F3 (NETZSCH). Two samples S1 (PG:RH = 2:1) (mass ratio) and S2 (PG:RH:SL = 5:2:1) (mass ratio), each about 10mg, are loaded into an $Al_2O_3$ crucible, respectively. From around 30°C to 1200°C, heating is carried out at 10, 15, and 20°C/min with 50 mL/min of $N_2$. Based on the literature, the kinetic characteristics of PG, including the starting decomposition temperature ($T_i$) and the peak temperature ($T_p$), are examined at 20°C/min.[23]

## 2.4 | Determination of product composition

The barium sulfate precipitation technique (GB/T 5484-2012) is used to determine the $CaSO_4$ concentration in PG. CaS is identified by spectrophotometric method (HJ 1226-2021). PG decomposition rate and CaS yield are calculated by Equations (1) and (2), respectively. The composition of the physical phase is identified by XRD. Scanning electron microscopy (SEM) is used to determine the surface morphology of the goods. The gas composition is determined using Agilent 7890B. Composition structure of tar is analyzed semi-quantitatively using a 300-MS GC/MS analyzer from VARIAN, USA, and classified into monocyclic aromatic hydrocarbons (MAHs), aliphatic hydrocarbons (AHs), nitrogen oxide-containing compounds (NOCs), phenols (Phenols), and polycyclic aromatic hydrocarbons (PAHs) based on the structural composition of each substance.

$$\varphi_{CaSO_4} = \frac{m_{o,CaSO_4}\text{-}m_{t,CaSO_4}}{m_{o,CaSO_4}} \times 100\% \tag{1}$$

$$\phi_{CaS} = \frac{m_{t,CaS}}{Q_{CaS}} \times 100\% \tag{2}$$

where $\varphi_{CaSO_4}$ denotes the PG decomposition rate, %; $m_{t,CaS}$ and $m_{t,CaSO_4}$ denote the quality of CaS and $CaSO_4$ in the product, respectively, g; $m_{o,CaSO_4}$ denotes the quality of $CaSO_4$ in PG, %; $Q_{CaS}$ denotes the theoretical quality of $CaSO_4$ converted to CaS completely, g; and $\phi_{CaS}$ denotes the CaS yield, %.

The theoretical decomposition rate of $CaSO_4$ and the theoretical yield of CaS have been calculated by converting SL to RH when the interaction between RH and SL is not considered. The calculation equation is as follows. The calculation equation is as follows.

$$\varphi_{CaSO_4-\mathrm{Theoretical}} = \varphi_{RH,CaSO_4} + \varphi_{SL,CaSO_4} \tag{3}$$

$$\phi_{CaS-\mathrm{Theoretical}} = \phi_{RH,CaS} + \phi_{SL,CaS} \tag{4}$$

where $\varphi_{CaSO_4-\mathrm{Theoretical}}$ represents the theoretical PG decomposition rate, %; $\varphi_{RH,CaSO_4}$ represents the PG decomposition rate during the reduction by RH alone, %; $\varphi_{SL,CaSO_4}$ represents the PG decomposition rate during the reduction by SL alone, %; $\phi_{CaS-\mathrm{Theoretical}}$ represents the theoretical yield of CaS, %; $\phi_{RH,CaS}$ represents the yield of CaS during the reduction by RH alone, %; and $\phi_{SL,CaS}$ represents the yield of CaS during the reduction by RH alone, %.

The char, tar, and gas yields are calculated according to Equation (5).

$$Yield = \frac{M_x}{M_{RH}} * 100\% \tag{5}$$

The equation $M_x$ is the yield of char, tar, and gas after the reduction of PG by RH and SL, g; $M_{RH}$ is the amount of RH and SL added, g.

The effect of RH and SL on PG decomposition behavior is investigated by six sets of experiments as shown in Table 4.

## 3 | RESULTS AND DISCUSSION

### 3.1 | Thermodynamic analysis

The main chemical reactions occurring during PG decomposition are calculated with FactSage, as shown in Table 5. First, $CaSO_4$ starts to decompose spontaneously at 1662°C with a high decomposition temperature. The addition of reducing agent significantly reduces the decomposition temperature of $CaSO_4$. Second, Figure 1 shows that the reactions of R1–R6 can all occur spontaneously, demonstrating that both gas–solid and solid–solid processes can drive PG decomposition.

**TABLE 5** Possible reactions during the reduction of PG by RH and SL.

| Number | Equation | Spontaneous reaction temperature (°C) |
|---|---|---|
| R1 | $CaSO_4 + 2C{=}CaS + 2CO_2(g)$ | 207.18 |
| R2 | $CaSO_4 + 5/2C{=}CaS + 3/2CO_2(g) + CO(g)$ | 304.19 |
| R3 | $CaSO_4 + 4C{=}CaS + 4CO(g)$ | 451.64 |
| R4 | $CaSO_4 + 4CO(g) = CaS + 4CO_2(g)$ | 0 |
| R5 | $CaSO_4 + CH_4(g) = CaS + 2H_2O(g) + CO_2(g)$ | 286.39 |
| R6 | $CaSO_4 + 4H_2(g) = CaS + 4H_2O(g)$ | 0 |
| R7 | $CaSO_4 = CaO + SO_2(g) + 1/2O_2(g)$ | 1661.92 |

### 3.2 | Influence of proportioning

The effects of RH and SL addition on decomposition rate of PG and CaS yield are investigated at 900°C for 30 min as shown in Figure 2a. When RH alone is used as the reducing agent, the decomposition rate increases from 25.87% to 99.99% with RH addition increasing from 10% to 50%. Decomposition rate remains the same when the RH content continues to be increased. This indicates that PG has been completely decomposed when 50% RH is added. When keeping the RH addition amount constant, the addition of SL can significantly increase the PG decomposition rate. For example, keeping the amount of 40% RH addition constant, the decomposition rate increases from 85.87% to 99.99% with SL addition increasing from 0% to 20%, which indicates that PG has been completely decomposed. In addition, by comparing the actual and theoretical decomposition rates, the predicted decomposition rate is clearly lower than the actual value

**TABLE 4** Experimental conditions for the reaction of PG with RH and SL.

| Number | Proportion | Temperature (°C) | Reaction time (min) |
|---|---|---|---|
| 1 | RH: PG = 10%–60% | 900 | 30 |
| 2 | RH:SL:PG = (10%–60%):(10%–20%):1 | 900 | 30 |
| 3 | RH: PG = 50% | 800–950 | 30 |
| 4 | RH:SL:PG = 40%:20%:1 | 800–950 | 30 |
| 5 | RH: PG = 50% | 900 | 10–40 |
| 6 | RH:SL:PG = 40%:20%:1 | 900 | 10–40 |

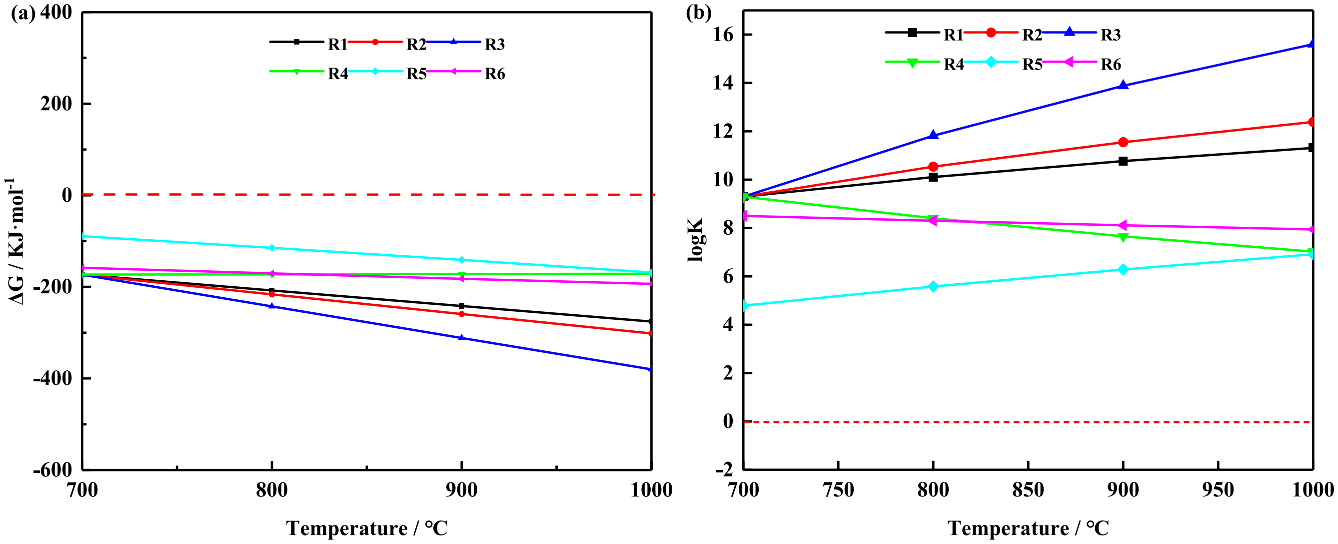

**FIGURE 1** (a) ΔG and (b) logK as a function of temperature for each reaction.

with the same SL addition. For example, the actual decomposition rate of 10% RH + 20% SL for PG is 56.38%, while the theoretical decomposition rate is only 48.67%; 40% RH + 20% SL for PG is 99.99%, while the theoretical decomposition rate is 94.38%. This suggests that the presence of interaction between RH and SL favors an increase in decomposition rate. When the addition of RH continues to increase to 50%, both the theoretical and actual decomposition rates have reached 99.99%, and PG has been completely decomposed. From Figure 2b, the theoretical CaS yield is inferior to the actual value under the same conditions. For example, the yield of 10% RH + 20% SL for CaS is 52.43%, while the theoretical decomposition rate is only 46.37%; 40% RH + 20% SL for CaS is 98.38%, while the theoretical decomposition rate is 95.21%. When the RH addition is 50%, the theoretical decomposition rate has reached 99.99%, and the actual decomposition rate is inferior to the theoretical value due to the measurement error. In addition, the difference between the values of CaS yield and decomposition rate is not significant, which indicates that the reduction product of $CaSO_4$ is CaS and almost no CaO is generated during the reduction reaction. The products are characterized by XRD as shown in Figure 2c. From Figure 2c, characteristic peaks of 40% RH + 20% SL and 50% RH are consistent, $CaSO_4$ has been completely reduced to CaS, and no obvious characteristic peaks of CaO, $Ca_2Al_2SiO_7$, and $Ca_2SiO_4$ are seen, which may be due to the low reaction temperature, $CaSO_4$ does not react with CaS to form CaO.[10] This indicates that the above CaS yield data are feasible.

PG:RH = 2:1 (S1) and PG:RH:SL = 5:2:1 (S2) are chosen as the best ratios. Because decomposition rate of S1 and S2 have reached 99.99% at 900°C. In addition, the experimental fixed PG dosage is 8 g. According to the ratios of S1 and S2, the amount of RH added in S1 is 4 g, and the amounts of RH and SL added in S2 are 3.2 g and 1.6 g. According to the results in Table 2, the fixed carbon content of RH is 2.91 times that of SL, respectively, so 1.6 g of SL can be converted into 0.55 g of RH according to the ratio of fixed carbon. So the total amount of RH added in S2 is 3.75 g, which is slightly lower than the RH content in S1. Despite the reduced RH content, the decomposition rate of PG still reached 99.99%. This result can also indicate that the interaction between SL and RH can improve the PG decomposition rate.

## 3.3 | Effect of temperature

Figure 3 depicts the effect of S1 and S2 on the PG decomposition process at various temperatures for 30 min. Increasing the temperature facilitates an increase in PG decomposition rate. The reaction process benefits from raising the temperature since the reduction of PG by RH and SL primarily involves linked gas–solid and solid–solid phase decompositions and is kinetically regulated. In addition, decomposition rate of S2 is superior to that of S1 below 900°C. For example, the decomposition rate of S2 is 80.05% significantly higher than that of S1 at 74.77% at 800°C, which shows that the presence of interaction between RH and SL favors an increase in decomposition rate. The decomposition rate of both S1 and S2 has reached 99.99% at 900°C. The decomposition rates do not change much when the temperature continues to increase. From Figure 3b, CaS yield increases with

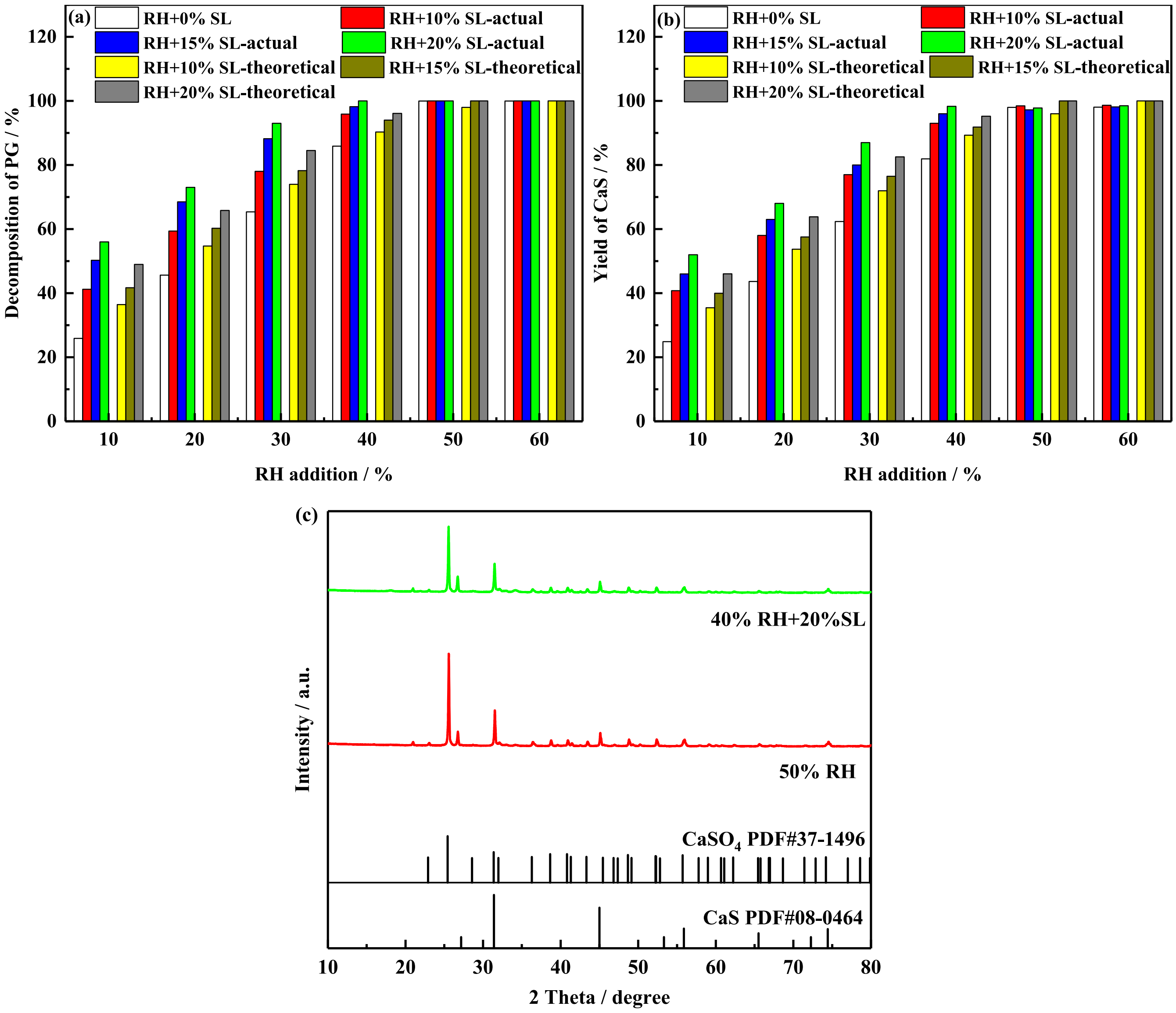

FIGURE 2 Effect of RH and SL addition on (a) PG decomposition rate; (b) CaS yield; (c) XRD patterns of the products.

increasing temperature and reaches 97.87% and 98.38% at 900°C for S1 and S2, respectively. In addition, the CaS yield is slightly lower than the PG decomposition rate, probably due to the measurement error, which indicates that the main decomposition product of $CaSO_4$ is CaS. Previous studies showed that there is a competitive reaction between CaS and CaO generation. CaS is produced in preference to CaO at 800–900°C.[24] From Figure 3c, $CaSO_4$ peak intensity in the products of S2 is weaker than that of S1 at 800°C, which proves that the decomposition rate of S2 is superior to that of S1. Furthermore, the products of S1 and S2 are mainly CaS, $CaSO_4$ has been completely consumed, and no obvious characteristic peak of CaO is found at 900°C.

## 3.4 | Effect of reaction time

The effect of S1 and S2 on the PG decomposition process is studied at different time at 900°C, as shown in Figure 4. Prolonging the reaction time favors an increase in the decomposition rate. Furthermore, the decomposition rate of S2 is superior to that of S1 for less than 30 min, which shows that the presence of interaction between RH and SL favors an increase in decomposition rate. The decomposition rate of both S1 and S2 has reached 99.99% for 30 min. From Figure 4b, CaS yield increases with time. CaS yield of S2 is superior to that of S1 for less than 30 min. From the XRD results in Figure 4c, the intensity of $CaSO_4$ peak in S1 reaction

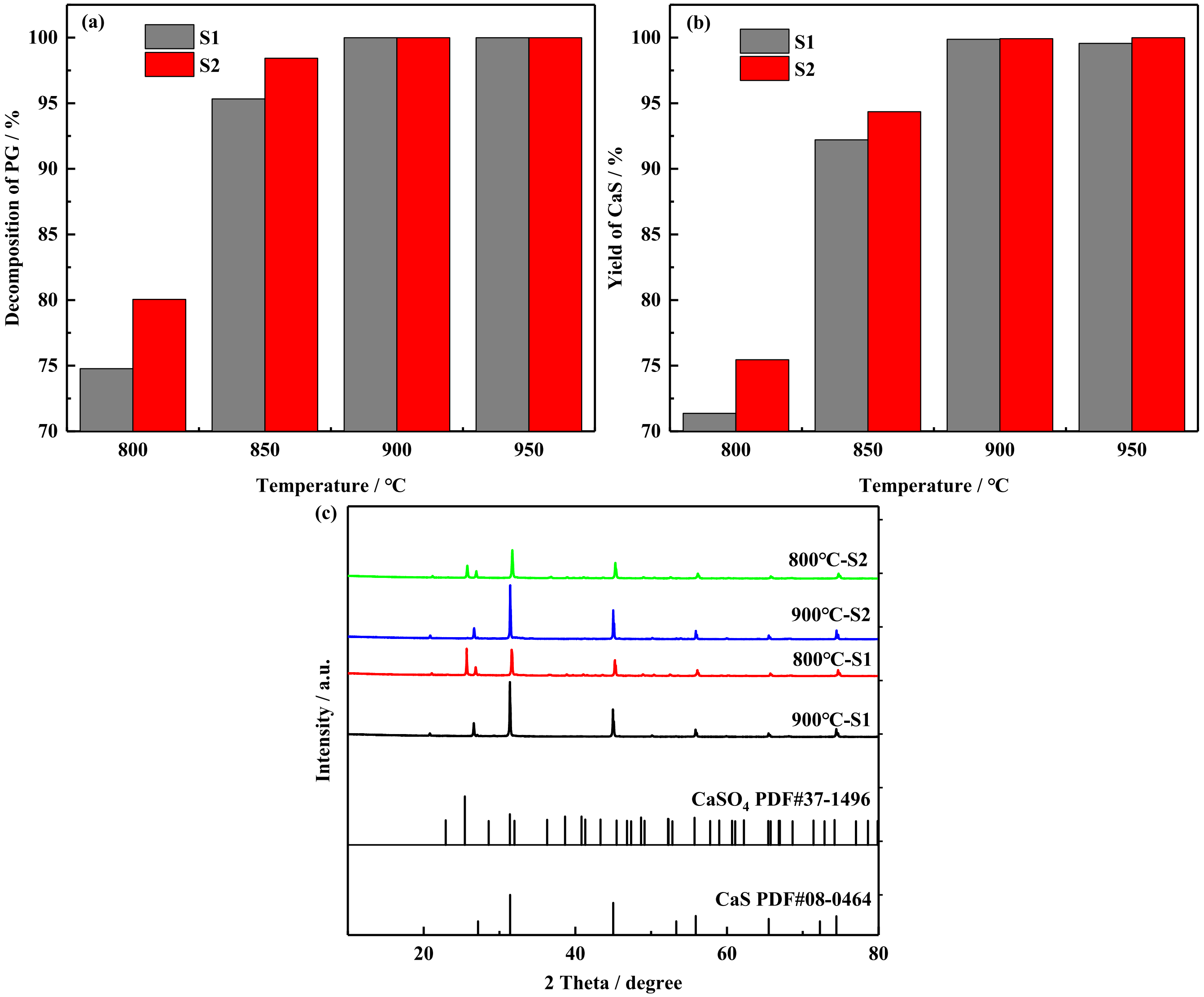

FIGURE 3 Effect of temperature on (a) PG decomposition rate; (b) CaS yield; (c) XRD pattern of the products.

product at 10min is significantly stronger than that of S2, which proves that the decomposition rate of S2 is superior to that of S1. Furthermore, solid phase products after S1 and S2 reaction are mainly CaS and unreacted $SiO_2$, and $CaSO_4$ has been completely consumed at 30 min.

## 3.5 | Thermogravimetric analysis

Figure 5 shows the TG-DTG curves of S1 and S2 at 20°C/min. From Figure 5a,b, three different weight loss processes occur at 30–200°C, 300–400°C, and 900–1000°C during PG decomposition. The first weightlessness is the precipitation of crystallized water in PG, RH, and SL. The second weightlessness is the pyrolysis of RH and SL to produce gases and tar. The third weightlessness is the reaction of PG with carbon and CO to produce CaS and CaO. Comparing Figure 5a,b, initial decomposition temperatures of S1 and S2 are 830.07°C and 810.06°C, respectively, corresponding to the third peak DTG curve temperatures of 980.47°C and 968.16°C. This suggests that RH and SL are more effective than RH alone in lowering the decomposition temperature of PG. Furthermore, S1's residual mass is smaller than S2's. This is due to the high SL ash content in S2.

## 3.6 | Calculation of kinetic parameters

Figure 6 depicts the TG-DTG curves of S1 and S2 at various heating rates. As the heating rate rises, the TG and DTG curves move to the right. Because increasing heating rate results in a shortening of the heat transfer time thus alleviating the thermal delay. Furthermore, when

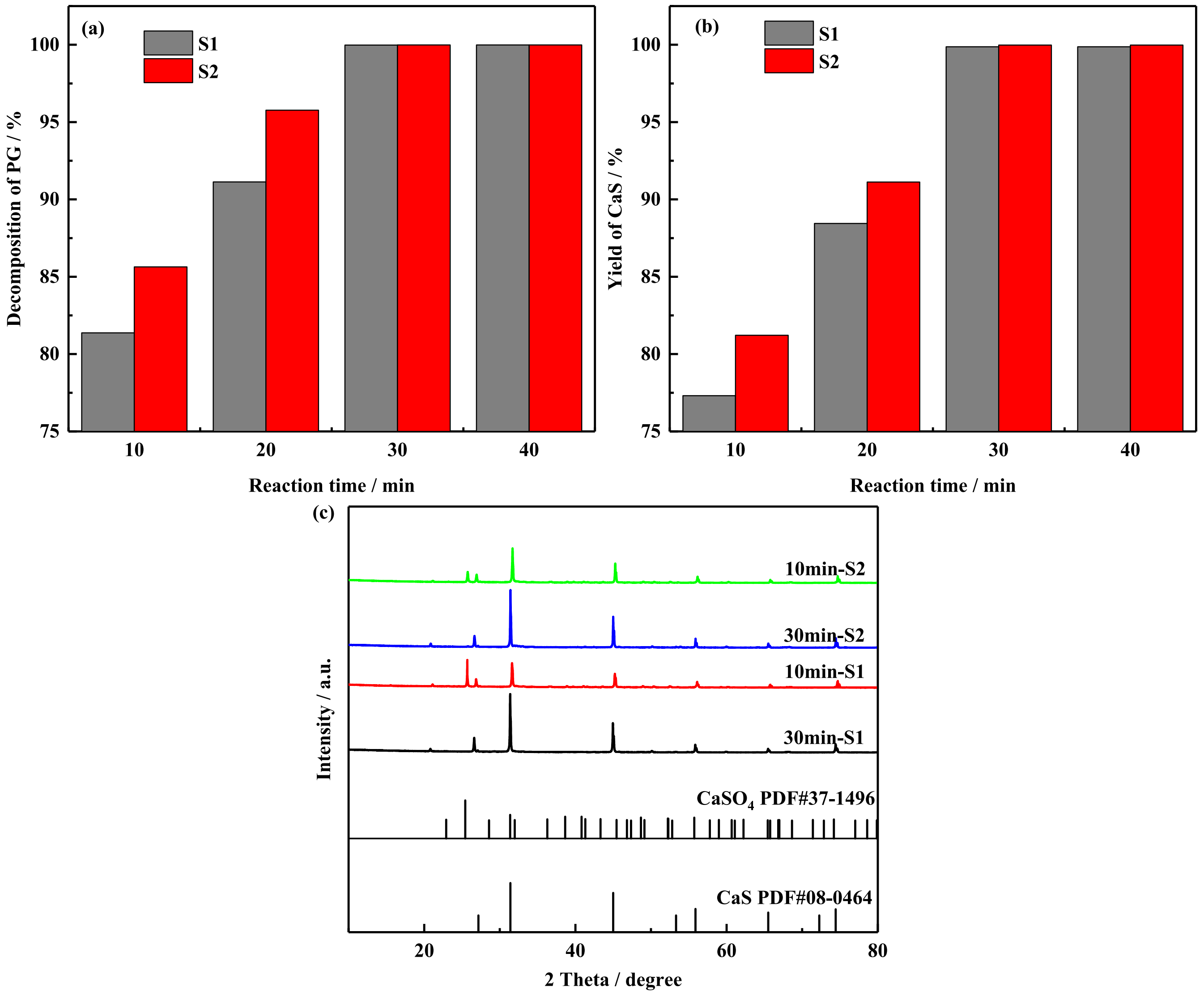

**FIGURE 4** Effect of reaction time on (a) PG decomposition rate; (b) CaS yield; (c) XRD patterns of the products.

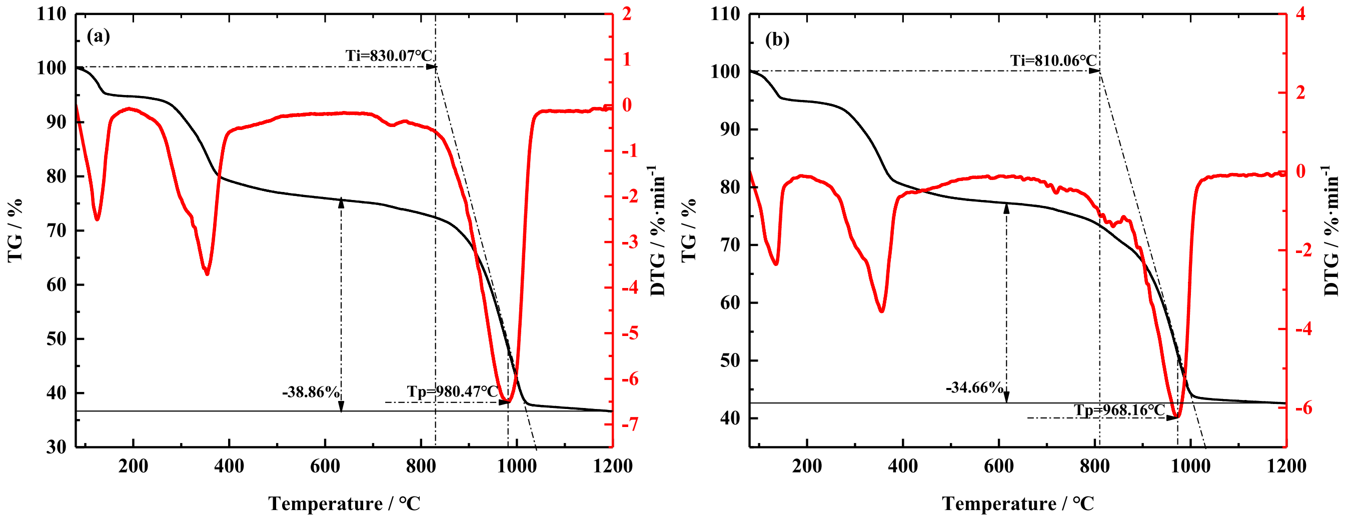

**FIGURE 5** TG-DTG curves of (a)S1 and (b)S2 at 20°C/min.

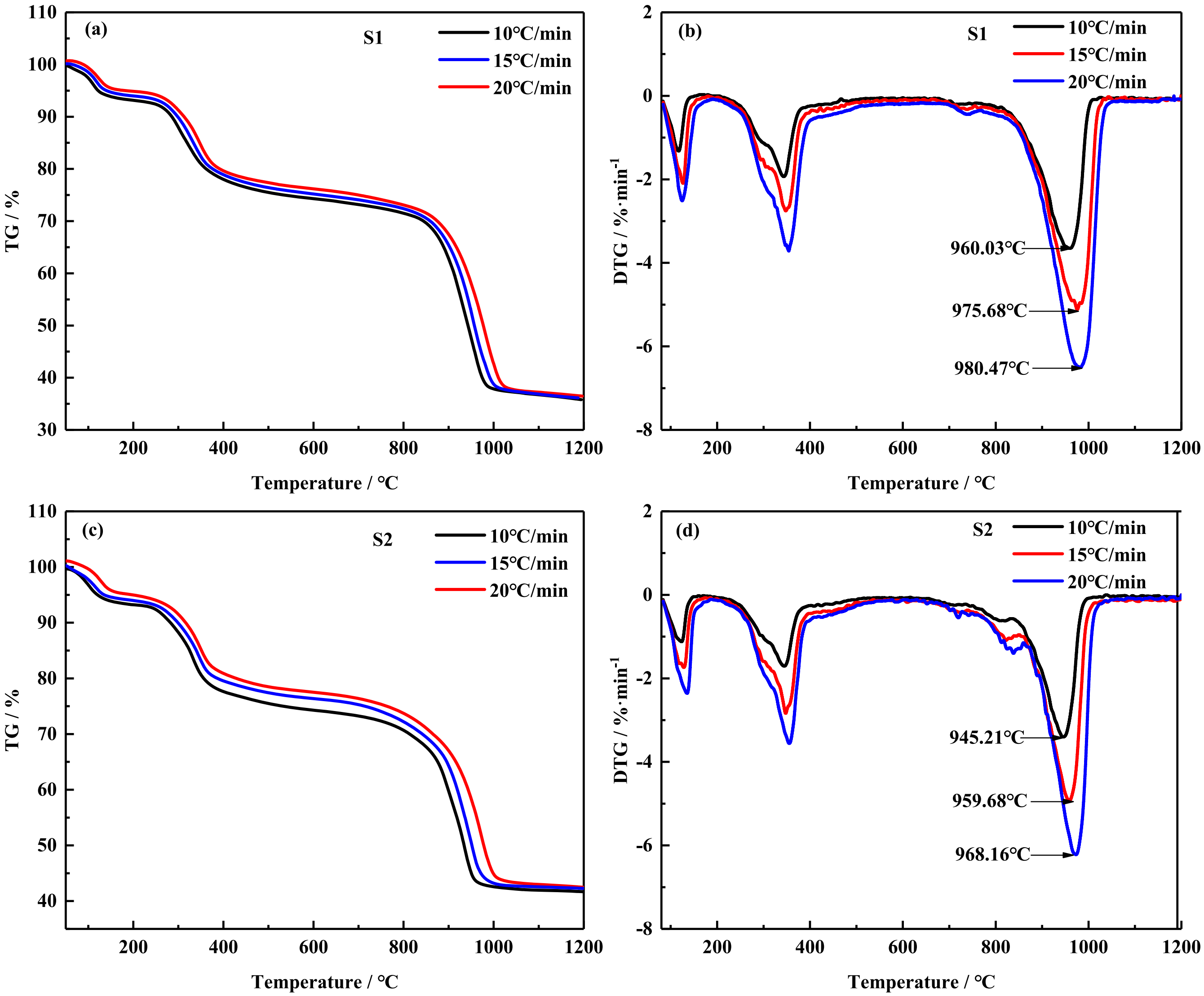

**FIGURE 6** TG-DTG curves of (a, b)S1 and (c, d)S2 at 10°C/ min, 15°C/ min and 20°C/min.

the heating rate increases, so does the maximum mass change rate. Because a faster heating rate allows more energy to be absorbed by the sample under the same circumstances, the activity of the reaction increases.[25] In addition, compared with Figure 6b,d, the third DTG peak temperature of S1 and S2 are 960.03°C, 975.68°C, 980.47°C and 945.21°C, 959.68°C, 968.16°C at 10, 15, and 20°C/min, respectively. The results show that the compound reductant is better than the single reductant in reducing the decomposition temperature of PG.

The kinetic characteristics of the PG breakdown process, including activation energy ($E_a$) and pre-exponential factor (lnA), are computed at 800–1000°C using the Flynn–Wall–Ozawa (FWO) and Kissinger–Akahira–Sunose (KAS) methods. Figure 7a,c demonstrates the association between ln(β) and 1/T with FWO for S1 and S2, respectively. Figure 7b,d demonstrates the connection between $\ln(\beta/T^2)$ and 1/T with the KAS for S1 and S2, respectively. The $R^2$ of the two models are 0.95–0.99 and 0.97–0.99, respectively, which indicates that the fit is satisfactory. In addition, calculations are performed for $E_a$ and lnA at each conversion rate (0.1–0.9) and the results are shown in Table 6. $E_a$ decreases with increasing conversion α because PG decomposition is a heat-absorbing process that requires progressively less energy as the temperature increases. Because a different approximation formula is chosen for P(x) resulting in a slightly higher $E_a$ calculated by FWO than KAS.[26] The $E_a$ calculated with FWO and KAS for S1 and S2 range from 349.33 to 540.42 kJ/mol, 340.89 to 531.21 kJ/mol and 324.33 to 515.42 kJ/mol, 315.89 to 506.21 kJ/mol, respectively. Comparing the $E_a$ calculated with FWO and KAS for the reduction of PG by S1 and S2, it is found that the $E_a$ required for S2 is lower than that for S1 at any conversion

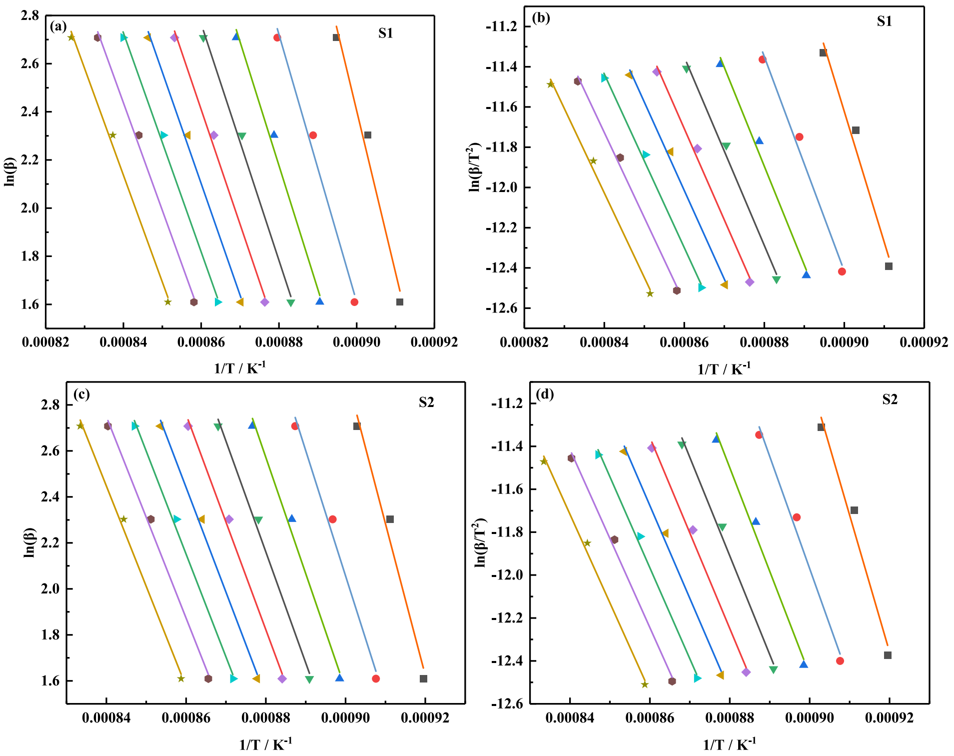

**FIGURE 7** (a) FWO and (b) KAS of S1; (c) FWO and (d) KAS of S2.

rate. This suggests that the interaction between RH and SL reduces the $E_a$ for PG decomposition at different heating rates. Furthermore, $E_a$ for both S1 and S2 is positively correlated with lnA. This is the result of a dynamic compensation effect.[27]

Because $E_a$ drops as the conversion rate (α) increases in Table 6, α1 of 0.5 is selected as the midway. Following the computation technique (see Supporting Information), $E_a$ is introduced into the equation at each step to produceG(α)/G(α1). Table S1 shows the selection of 15 typical kinetic mechanism functions G(α).[28] Figure 8 is the result of mathematical processing. The link between mechanism function G(α)/G(α1) and α is depicted on the left axis. The fluctuation of the experimental findings $P\ (X_\alpha)/P(X_{\alpha 1})$ with α is shown on the right axis.[29] The two curves are compared at different conversion rates to determine the most likely mechanism function G(α).

Figure 8 shows that the experimental results of S1 and S2 agree well with the mechanism function $G(\alpha) = -\ln(1-\alpha)$. This suggests that the decreased PG processes in S1 and S2 are compatible with the nucleation and growth paradigm. This conclusion is congruent with those of Antar[17,29]and Liu.[18] Based on this model, it can be postulated that at room temperature, PG is in contact with the reducing agent. When it reaches about 800°C, the PG is gradually reduced. CaS nuclei are formed and increased progressively, and the created gas diffuses from within to outside, resulting in the construction of pore structure on the product surface.[30] From Figure 9, many small pores appear on the surface of the PG after the reaction, which are caused by the escape of the gas.

## 3.7 | Analysis of the synergistic mechanism

From the above study, it can be found that the mineral fraction in SL, such as $Fe_2O_3$, with significant catalytic activity can promote the increase of PG decomposition rate. The impact of SLA on PG decomposition is examined to better understand the mechanism, as seen in Figure 10. According to Figure 10a, increasing the SL and SLA additions from 0% to 10%, respectively, results in an increase in the PG decomposition rate from 91.87% to 99.99% and from 91.87% to 97.84%. The rate of PG decomposition after adding SLA is lower than that of SL under the same circumstances. This is due to the fact that SL contains volatile fraction, and SL pyrolysis can produce reducing gas, which favors to PG decomposition. In addition, the addition of SLA also increase the decomposition rate. The RH pyrolysis tar may break as a result of reactive chemicals like $Fe_2O_3$ in the SL, increasing the amount of reducing gas and speeding up the pace at which PG decomposes. The findings are congruent with those of Song et al.[31] and Gao et al.[22]

To further investigate the changes of crystals in the solid particles, SL, post-reaction SL, SLA, and post-reaction SLA are characterized by XRD as shown in

**TABLE 6** FWO and KAS estimate the $E_a$, lnA and $R^2$ of S1 and S2.

| Sample | S1 | | | | | | | | S2 | | | | | | | |
|---|---|---|---|---|---|---|---|---|---|---|---|---|---|---|---|---|
| | FWO | | | | KAS | | | | FWO | | | | KAS | | | |
| α | lnA $(min^{-1})$ | $R^2$ | $E_a$ (kJ/mol) | $R^2$ | lnA $(min^{-1})$ | $R^2$ | $E_a$ (kJ/mol) | $R^2$ | lnA $(min^{-1})$ | $R^2$ | $E_a$ (kJ/mol) | $R^2$ | lnA $(min^{-1})$ | $R^2$ | $E_a$ (kJ/mol) | $R^2$ |
| 0.1 | 55.71 | 0.95 | 540.42 | 0.95 | 54.91 | 0.95 | 531.21 | 0.95 | 52.71 | 0.97 | 515.42 | 0.97 | 51.91 | 0.97 | 506.21 | 0.97 |
| 0.2 | 44.54 | 0.96 | 442.96 | 0.96 | 43.92 | 0.96 | 434.83 | 0.96 | 41.54 | 0.98 | 417.96 | 0.98 | 40.91 | 0.99 | 409.83 | 0.99 |
| 0.3 | 40.90 | 0.98 | 408.34 | 0.98 | 40.09 | 0.99 | 404.12 | 0.99 | 37.90 | 0.99 | 383.34 | 0.99 | 37.09 | 0.99 | 379.12 | 0.99 |
| 0.4 | 38.88 | 0.99 | 389.02 | 0.99 | 37.97 | 0.99 | 381.91 | 0.99 | 35.88 | 0.99 | 364.01 | 0.99 | 34.97 | 0.99 | 356.91 | 0.99 |
| 0.5 | 37.60 | 0.99 | 376.63 | 0.99 | 36.60 | 0.99 | 370.28 | 0.99 | 34.60 | 0.99 | 351.62 | 0.99 | 33.60 | 0.99 | 345.28 | 0.99 |
| 0.6 | 36.50 | 0.99 | 365.91 | 0.99 | 35.43 | 0.99 | 360.23 | 0.99 | 33.50 | 0.99 | 340.91 | 0.99 | 32.43 | 0.99 | 335.23 | 0.99 |
| 0.7 | 35.79 | 0.99 | 358.82 | 0.99 | 34.67 | 0.99 | 350.62 | 0.99 | 32.79 | 0.99 | 333.81 | 0.99 | 31.67 | 0.99 | 325.62 | 0.99 |
| 0.8 | 35.06 | 0.99 | 351.29 | 0.99 | 33.89 | 0.99 | 342.61 | 0.99 | 32.06 | 0.99 | 326.29 | 0.99 | 30.89 | 0.99 | 317.61 | 0.99 |
| 0.9 | 34.94 | 0.99 | 349.33 | 0.99 | 33.74 | 0.99 | 340.89 | 0.99 | 31.94 | 0.99 | 324.33 | 0.99 | 30.74 | 0.99 | 315.89 | 0.99 |

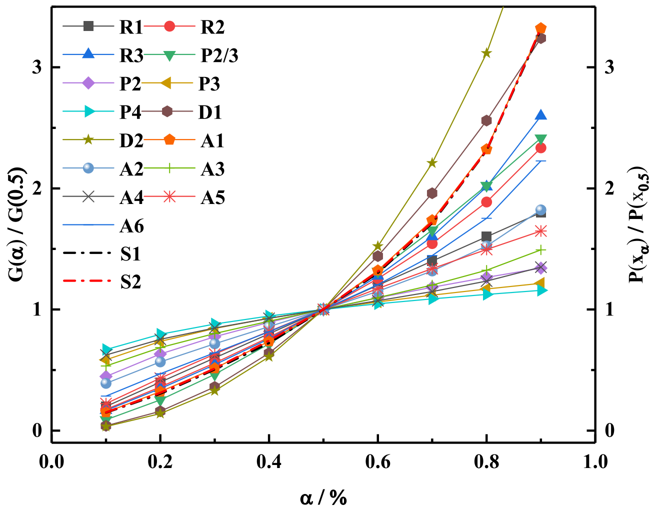

**FIGURE 8** Variation of G(α)/G(0.5) and $P(X_α)/P(X_{0.5})$ with conversion for different reaction models.

Figure 10b. The main mineral components in the SL and SLA are $SiO_2$ and $Fe_2O_3$, both of which have similar compositions. Therefore, calcination does not change the mineral composition of the SL. Therefore, it is feasible to use SLA instead of SL to investigate the influence of mineral composition in SL on PG decomposition process. For the reacted SL and SLA, characteristic peaks of $Fe_3O_4$, FeO, $Fe_2SiO_4$, and Fe appear in the products. According to the XRD results, the reduction process of iron oxides in SL can be summarized as $Fe_2O_3 \rightarrow Fe_3O_4$/FeO → Fe.[32] Since the reaction temperature is 900°C, FeO will continue to react with $SiO_2$ at high temperature to form $Fe_2SiO_4$. $Fe_2O_3$ reduction can be understood as the consumption of reactive oxygen in $Fe_2O_3$. The reactive oxygen on the surface of $Fe_2O_3$ can be divided into lattice oxygen and chemisorbed oxygen, both of which are capable of partial oxidation reaction with coal tar and promote the cracking of tar to produce small molecule gases, such as CO and $H_2$. When the reactive oxygen on the surface reacts with the tar molecule, oxygen vacancies are formed on $Fe_2O_3$. The lattice oxygen in the bulk phase of $Fe_2O_3$ migrates to the surface to replenish the consumed reactive oxygen. As the reaction proceeds, when the lattice oxygen in the bulk phase is not sufficient to replenish the consumed surface active oxygen, $Fe_2O_3$ undergoes a significant iron species transformation and is eventually converted to $Fe_3O_4$, FeO, and Fe.[33]

The gas composition after the reaction is measured as shown in Figure 10c. The addition of SL to RH can significantly increase the content of reducing gases CO, $CH_4$, and $H_2$. For example, increasing the SL addition from 0% to 10% raises the CO content from 32.99 to 38.08 mL/g and the $H_2$ content from 23.49 to 32.48 mL/g.

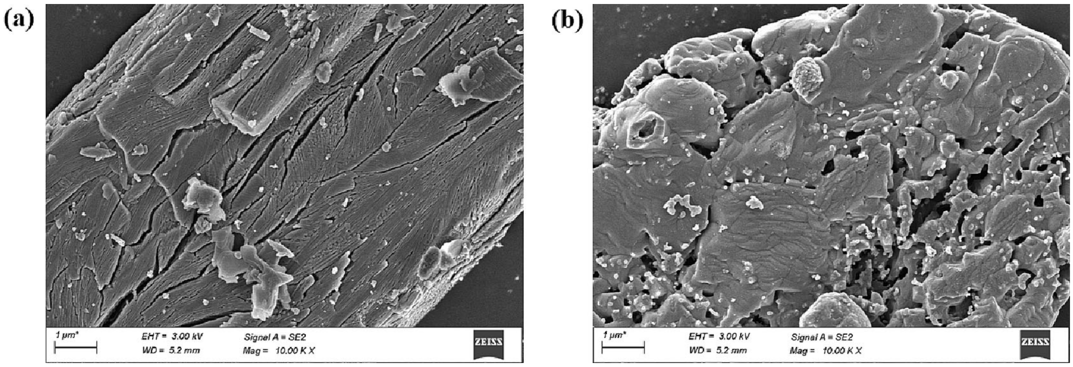

FIGURE 9 Surface of (a) PG; (b) postreaction product.

Furthermore, the $CO_2$ level rises from 385.57 to 492.24 mL/g. The increase of $CO_2$ concentration is caused by the reaction of R1, R2, R4, and R5. $CO_2$ concentrations are rising as a result of CO depletion. However, SL pyrolysis produces reducing gas, which raises the overall amount of gas since the amount produced exceeds the amount consumed. Since SLA pyrolysis does not produce reducing gases, the gas composition after adding SLA reflects the process of gas participation in chemical reactions. Furthermore, as SLA concentration rises from 0% to 10%, the CO content falls from 32.99 to 26.88 mL/g, the $H_2$ content falls from 23.49 to 15.68 mL/g, the $CH_4$ content falls from 14.68 to 10.08 mL/g, and the $CO_2$ concentration rises from 385.57 to 405.92 mL/g. The reduction of PG to CaS by reducing gases leads to the decrease in concentration. In addition, the reduction of $Fe_2O_3$ also consumes part of the reducing gas.

The tar composition after the reaction is determined by GC-MS as shown in Figure 10d. The addition of SLA changes the tar composition. For example, when the amount of SLA added is increased from 0% to 10%, the MAHs content in the tar increases from 21.19% to 31.04%, the AHs content increases from 2.31% to 10.74%, the PAHs content decreases from 11.85% to 7.23%, the Phenols content decreases from 31.96% to 26.87%, and the NOCs decreases from 33.19% to 24.12%. The reason is that $Fe_2O_3$ promotes the breakage of C-O and C-C bonds, which can convert NOCs as well as PAHs into lighter components and promote the production of AHs and MAHs[34,35] while generating CO, $H_2$, and $CH_4$ gases. In addition, $Fe_2O_3$ promotes the occurrence of dephenolization of hydroxyl groups, leading to a decrease in the content of Phenols. It is found that $Fe^{3+}$ uses some of its d-vacancy orbitals to bind to oxygen-containing functional groups in tar or π-bonds in unsaturated hydrocarbons, which promotes the breakage between chemical bonds and the decomposition of Phenols or NOCs to form MAHs.[36]

In addition, the yields of char in the products after the reduction of PG by 40% RH, 10% SL and 40% RH + 10% SL are investigated, and the results are shown in Figure 11e. The yield of char after reduction of PG by RH and SL alone is 14.38% and 56.42%, respectively, and the sum of the two is 70.80%. When the sum of char yield is 62.65% after the reduction of PG by RH and SL together, the char yield is significantly lower. This indicates that the ash in SL promotes the reaction process of carbon with $CaSO_4$. Figure 11f also supports this conclusion. The fixed carbon content in the char is 0.42 and 0.12 g for RH and SL reduction alone, respectively. The sum of the two is 0.54 g. When RH and SL are reduced together, the fixed carbon content in the char is 0.49 g, a significant reduction in fixed carbon content. It was shown that $SiO_2$, $Al_2O_3$, and $Fe_2O_3$ can significantly promote the reaction process of carbon and $CaSO_4$ and increase the decomposition rate of PG.[8]

Because the reducing gas will react with the PG to create $CO_2$, the gas composition in Figure 10 is unlikely to accurately reflect the catalytic action of $Fe_2O_3$ in SLA on the RH pyrolysis process. As a result, the link between the yield and gas composition of each RH pyrolysis product and the quantity of SLA added is explored by directly adding SLA to RH at 900°C for 30 min without adding PG, as shown in Figure 11.

Figure 11a shows that the gas yield steadily improves from 49.6% to 57.2%, the tar yield declines from 7.2% to 1.2%, and char yield do not change much. as SLA is increased from 0% to 10%. This suggests that the breaking of the tar increases the gas output.[37] This indicates that the active substances such as $Fe_2O_3$ in the SLA can play the effect of tar cracking. From Figure 11b,c, it can be found that increasing SLA addition can promote the increase of $CH_4$, CO, and $H_2$ production. The content of NOCs and PAHs in tar significantly decreases and the content of light components such as MAHs and AHs significantly increases. This is consistent with the

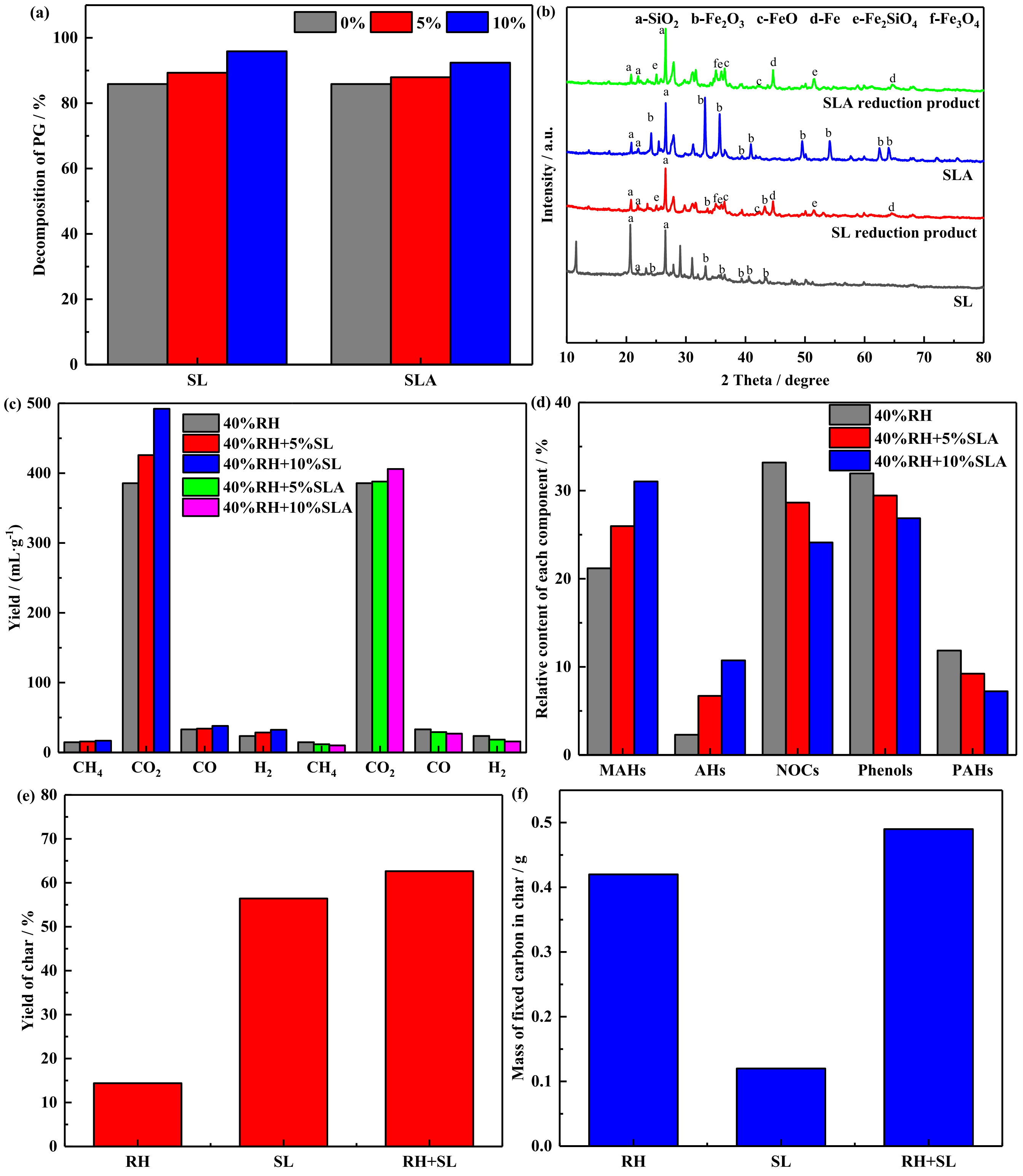

**FIGURE 10** Effect of SL and SLA addition on (a) PG decomposition rate; (b) XRD spectra of each substance; (c) gas composition; (d) tar composition; (e) char yield; (f) mass of fixed carbon in char (condition: 900°C, 30 min).

findings in Figure 10. It is possible that $Fe_2O_3$ causes a decrease in the $E_a$ required for C-O bond breaking, resulting in epoxy, carboxyl, and ether bond breakage.[38,39] Furthermore, $Fe_2O_3$ enhances the cleavage reaction of PAHs, resulting in a decrease in NOC and PAH content and an increase in MAHs and AHs, as

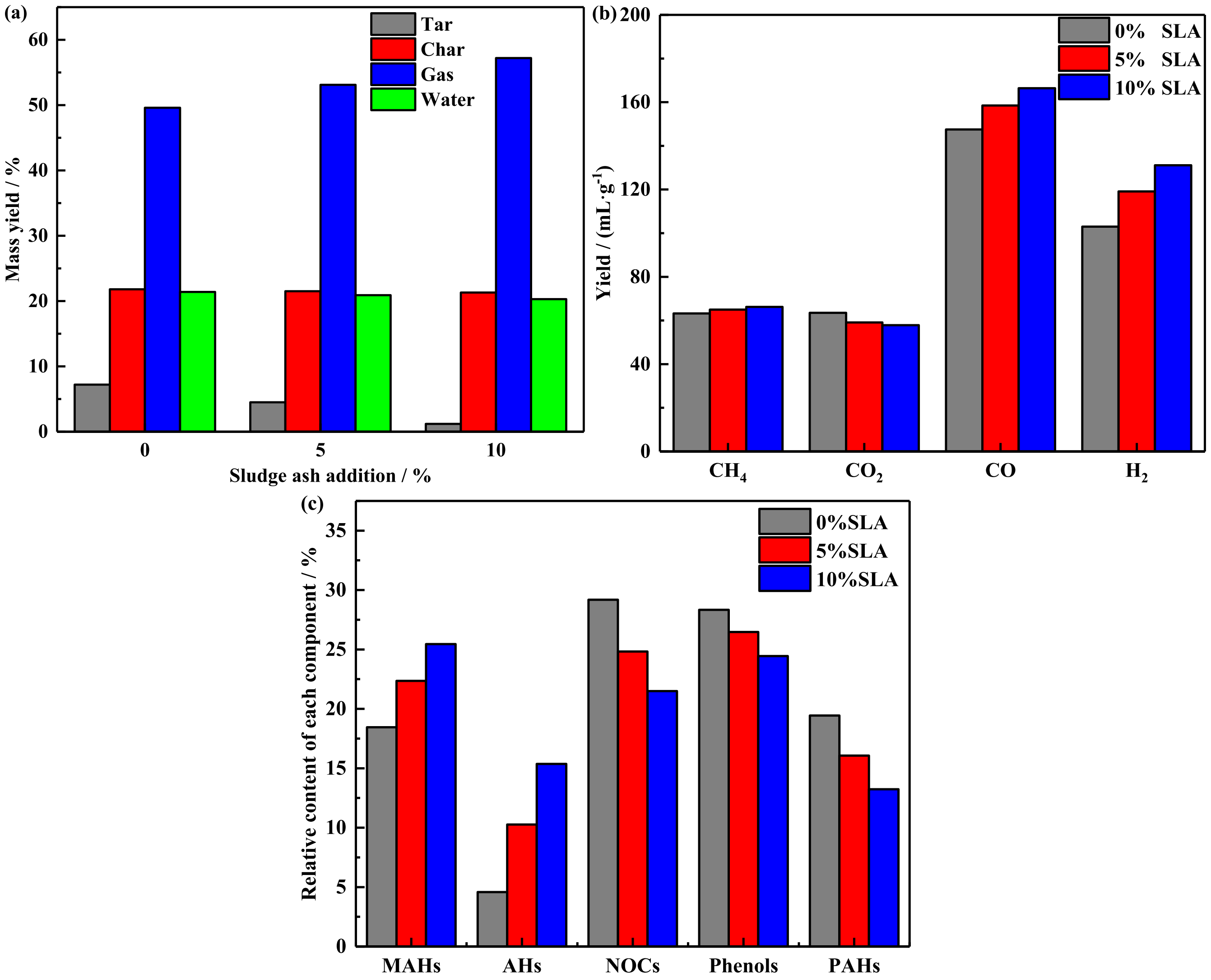

**FIGURE 11** Effect of SLA addition on (a) RH pyrolysis products; (b) gas composition; (c) tar composition (condition: 900°C, 30 min).

well as the formation of CO, $H_2$, and $CH_4$. The occurrence of the Boudouard reaction may be responsible for the reduction in $CO_2$ output.[40]

Finally, a synergistic reaction mechanism is proposed. First, the rapid pyrolysis of RH and SL at high temperature produces tar and gas. Because of the high concentration of active component $Fe_2O_3$ in SL, $Fe_2O_3$ promotes the breakdown of tar, converting NOCs and PAHs of tar into lighter components. The production of AHs and MAHs is promoted, while more CO, $H_2$, and $CH_4$ gases are produced. At the same time, $Fe_2O_3$ is reduced to $Fe_3O_4$, FeO, and Fe. In addition, the SLA significantly facilitates the reaction process of carbon with PG. In the presence of reducing gases and carbon, the PG decomposition reaction begins to occur. CaS nuclei are formed and eventually grow in size. The produced gas passes the sample surface, causing pore structures to develop.

## 4 | CONCLUSIONS

To solve the environmental problems caused by solid waste PG, SL-assisted RH reduction of PG to CaS is used. The experimental conditions are optimized and the synergistic mechanism is investigated by experimental studies and kinetic analysis. It is found that using 40% RH + 20% SL as a reducing agent for 30 min at 900°C results in a PG decomposition rate of 99.99% and a CaS yield of 98.38%. RH alone is less effective than RH + SL in lowering $E_a$ and the initial decomposition temperature. The nucleation and growth paradigm is supported by the mechanism functions of both reduced PG, which are $G(\alpha) = -\ln(1 - \alpha)$. There is a promotion effect between RH and SL. $Fe_2O_3$ in SL can promote the cracking of NOCs and PAHs in the tar leading to more CO, $H_2$, and $CH_4$ gas generation. Meanwhile, SLA can significantly promote the reaction process of carbon and $CaSO_4$, thus increasing the decomposition rate of PG. This study provides an idea for developing more economical and environmentally friendly reductant decomposition of PG.

## ACKNOWLEDGEMENTS

The authors would like to thank the financial support from the school-enterprise cooperation projects (No. 2019-KYY-508101-0078).

## CONFLICT OF INTEREST STATEMENT

This paper's authors declare no conflicts of interest.

## ORCID

*Dong Ma* https://orcid.org/0000-0002-6229-9971

## REFERENCES

1. Wei ZQ, Deng ZB. Research hotspots and trends of comprehensive utilization of phosphogypsum: bibliometric analysis. *J Environ Radioact*. 2022;242:106778. doi:10.1016/j.jenvrad.2021.106778
2. Lv XF, Xiang L. The generation process, impurity removal and high-value utilization of phosphogypsum material. *Nanomaterials*. 2022;12(17):3021. doi:10.3390/nano12173021
3. Xiao YD, Jin HX, Wang ML, Guo YL. Collaborative utilization status of red mud and phosphogypsum: a review. *J Sustain Metall*. 2022;8(4):1422-1434. doi:10.1007/s40831-022-00569-x
4. Wang Y, Wan TM, Zhong YJ, Ma XD, Chen ZY, Wang XL. Environmental sustainability of renewable phosphogypsum by CaS characterization and process optimization. *J Therm Anal Calorim*. 2020;139(6):3457-3471. doi:10.1007/s10973-019-08718-3
5. Pérez-López R, Macías F, Cánovas CR, Sarmiento AM, Pérez-Moreno SM. Pollutant flows from a phosphogypsum disposal area to an estuarine environment: an insight from geochemical signatures. *Sci Total Environ*. 2016;553:42-51. doi:10.1016/j.scitotenv.2016.02.070
6. Wu FH, Ren YC, Qu GF. Utilization path of bulk industrial solid waste: a review on the multi-directional resource utilization path of phosphogypsum. *J Environ Manage*. 2022;313:114957. doi:10.1016/j.jenvman.2022.114957
7. Yang H, Xu Y, Shen K, Qiu Y, Zhang G. Removal of heavy metal ions from zinc hydrometallurgical wastewater using CaS-containing alkaline slag. *J Environ Chem Eng*. 2018;6(5):6451-6456. doi:10.1016/j.jece.2018.09.040
8. Jia X, Wang Q, Cen K, Chen L. An experimental study of $CaSO_4$ decomposition during coal pyrolysis. *Fuel*. 2016;163:157-165. doi:10.1016/j.fuel.2015.09.054
9. Yang J, Ma LP, Zheng DL, Zhao SQ, Peng YH. Reaction mechanism for syngas preparation by lignite chemical looping gasification using phosphogypsum oxygen carrier. *Energy Fuel*. 2018;32(7):7857-7867. doi:10.1021/acs.energyfuels.8b01112
10. Bi YX, Xu L, Yang M, Chen QL. Study on the effect of the activity of anthracite on the decomposition of phosphogypsum. *Ind Eng Chem Res*. 2022;61(19):6311-6321. doi:10.1021/acs.iecr.2c00081
11. Zheng SC, Ning P, Ma LP, Cheng FX, Shi JY. Phosphogypsum as a raw material for the production of $SO_2$ and lime in circulating fluidized beds. *Combust Sci Technol*. 2014;186(3):377-386. doi:10.1080/00102202.2013.864286
12. Suslikov AV, Zhirnov BS, Murtazin FR. A study of the kinetics of the reaction of petroleum coke with phosphogypsum to give calcium sulfide. *Chem Technol Fuels Oils*. 2021;57(3):461-466. doi:10.1007/s10553-021-01266-3
13. Zhu K, Xie G, Chen Z, Wang Q. Reaction characteristics of phosphogypsum under carbon monoxide atmosphere. *J Chin Ceram Soc*. 2013;41(11):1540-1545.
14. Ren X, Xia J, Zhang Z. Thermodynamic analysis of reductive decomposition for phosphogypsum. *Chin J Environ Eng*. 2013;7(3):1128-1132.
15. Lian Y, Ma L, Liu H. Experimental study on preparation of calcium sulfide via phosphogypsum and hydrogen sulfide reaction. *Chem Eng (China)*. 2016;44(8):48-52. doi:10.3969/j.issn.1005-9954.2016.08.010
16. Zhang Y, Yang Q, Liu Y, Guo Q. TG-FTIR study on phosphogypsum reduction with lignite under $CO_2$ atmosphere. *J Chem Eng Chin Univ*. 2016;30(3):611-617.
17. Antar K, Jemal M. Recovery of calcium sulfide from Tunisian phosphogypsum and olive mill wastewaters: a thermogravimetric and kinetic study. *J Therm Anal Calorim*. 2022;147(5):3931-3946. doi:10.1007/s10973-021-10773-8
18. Liu Q, Ao XQ, Chen QL, Xie Y, Cao Y. Reaction characteristics and kinetics of phosphogypsum decomposition via synergistic reduction effect of composite reducing agent. *J Mater Cycles Waste Manage*. 2022;24(2):595-605. doi:10.1007/s10163-021-01344-y
19. Xiong Q, Wu X, Lv H, Liu SH, Hou HB, Wu X. Influence of rice husk addition on phosphorus fractions and heavy metals risk of biochar derived from sewage sludge. *Chemosphere*. 2021;280:130566. doi:10.1016/j.chemosphere.2021.130566
20. Chang SH. Rice husk and its pretreatments for bio-oil production via fast pyrolysis: a review. *Bioenergy Res*. 2020;13(1):23-42. doi:10.1007/s12155-019-10059-w
21. Song Q, Zhao HY, Xing WL. Effects of various additives on the pyrolysis characteristics of municipal solid waste. *Waste Manag*. 2018;78:621-629. doi:10.1016/j.wasman.2018.06.033
22. Gao NB, Sipra AT, Quan C. Thermogravimetric analysis and pyrolysis product characterization of municipal solid waste using sludge fly ash as additive. *Fuel*. 2020;281:118572. doi:10.1016/j.fuel.2020.118572
23. Xie T, Wei RC, Wang Z, Wang J. Comparative analysis of thermal oxidative decomposition and fire characteristics for different straw powders via thermogravimetry and cone calorimetry. *Process Saf Environ Prot*. 2020;134:121-130. doi:10.1016/j.psep.2019.11.028
24. Ma LP, Niu XK, Hou J, Zheng SC, Xu WJ. Reaction mechanism and influence factors analysis for calcium sulfide generation in the process of phosphogypsum decomposition. *Thermochim Acta*. 2011;526(1–2):163-168. doi:10.1016/j.tca.2011.09.013
25. Qu Y, Li A, Wang D, Zhang L, Ji G. Kinetic study of the effect of in-situ mineral solids on pyrolysis process of oil sludge. *Chem Eng J*. 2019;374:338-346. doi:10.1016/j.cej.2019.05.183
26. He Q, Ding L, Gong Y, Li W, Wei J, Yu G. Effect of torrefaction on pinewood pyrolysis kinetics and thermal behavior using

thermogravimetric analysis. *Bioresour Technol*. 2019;280:104-111. doi:10.1016/j.biortech.2019.01.138

27. Sobek S, Werle S. Isoconversional determination of the apparent reaction models governing pyrolysis of wood, straw and sewage sludge, with an approach to rate modelling. *Renew Energy*. 2020;161:972-987. doi:10.1016/j.renene.2020.07.112
28. Vyazovkin S, Chrissafis K, Di Lorenzo ML. ICTAC kinetics committee recommendations for collecting experimental thermal analysis data for kinetic computations. *Thermochim Acta*. 2014;590:1-23. doi:10.1016/j.tca.2014.05.036
29. Antar K, Jemal M. A thermogravimetric study into the effects of additives and water vapor on the reduction of gypsum and Tunisian phosphogypsum with graphite or coke in a nitrogen atmosphere. *J Therm Anal Calorim*. 2018;132(1):113-125. doi:10.1007/s10973-017-6871-6
30. Tian HJ, Guo QJ. Investigation into the behavior of reductive decomposition of calcium sulfate by carbon monoxide in chemical-looping combustion. *Ind Eng Chem Res*. 2009;48(12):5624-5632. doi:10.1021/ie900089m
31. Song Q, Zhao HY, Jia JW. Pyrolysis of municipal solid waste with iron-based additives: a study on the kinetic, product distribution and catalytic mechanisms. *J Clean Prod*. 2020;258:120682. doi:10.1016/j.jclepro.2020.120682
32. Lin BC, Huang QX, Yang YX, Chi Y. Preparation of Fe-char catalyst from tank cleaning oily sludge for the catalytic cracking of oily sludge. *J Anal Appl Pyrolysis*. 2019;139:308-318. doi:10.1016/j.jaap.2019.03.006
33. Wang DC, Jin LJ, Li Y. Integrated process of coal tar upgrading and in-situ reduction of $Fe_2O_3$. *Fuel Process Technol*. 2019;191:20-28. doi:10.1016/j.fuproc.2019.03.024
34. He L, Li SG, Lin WG. Catalytic cracking of pyrolytic vapors of low-rank coal over limonite ore. *Energy Fuel*. 2016;30(9):6984-6990. doi:10.1021/acs.energyfuels.6b01182
35. He L, Hui HL, Li SG, Lin WG. Production of light aromatic hydrocarbons by catalytic cracking of coal pyrolysis vapors over natural iron ores. *Fuel*. 2018;216:227-232. doi:10.1016/j.fuel.2017.12.005
36. Zhang X, Zhu J, Ban Y, Liu F, Jin L, Hu H. Effect of $Fe_2O_3$ on the pyrolysis of two demineralized coal using in-situ pyrolysis photoionization time-of-flight mass spectrometry. *J Fuel Chem Technol (Beijing, China)*. 2021;49(5):589-597. doi:10.1016/S1872-5813(21)60065-8
37. Zhang LX, Kudo S, Tsubouchi N, Hayashi J, Ohtsuka Y, Norinaga K. Catalytic effects of Na and Ca from inexpensive materials on in-situ steam gasification of char from rapid pyrolysis of low rank coal in a drop-tube reactor. *Fuel Process Technol*. 2013;113:1-7. doi:10.1016/j.fuproc.2013.03.009
38. Zhao HY, Li YH, Song Q. Effects of iron ores on the pyrolysis characteristics of a low-rank bituminous coal. *Energy Fuel*. 2016;30(5):3831-3839. doi:10.1021/acs.energyfuels.6b00061
39. Liu JW, Zhang Q, Liang LT, Guan GQ, Huang W. Catalytic depolymerization of coal char over iron-based catalyst: potential method for producing high value-added chemicals. *Fuel*. 2017;210:329-333. doi:10.1016/j.fuel.2017.08.074
40. Lin BC, Huang QX, Chi Y. Co-pyrolysis of oily sludge and rice husk for improving pyrolysis oil quality. *Fuel Process Technol*. 2018;177:275-282. doi:10.1016/j.fuproc.2018.05.002

## SUPPORTING INFORMATION

Additional supporting information can be found online in the Supporting Information section at the end of this article.

**How to cite this article:** Ma D, Wang Q, Tian Z. Preparation of calcium sulfide by sludge-assisted rice husk reduction of phosphogypsum. *Asia-Pac J Chem Eng*. 2023;18(4):e2915. doi:10.1002/apj.2915